Surface Chemistry

Deutsche Ausgabe: DOI: 10.1002/ange.201800673
Internationale Ausgabe: DOI: 10.1002/anie.201800673

"Precipitation on Nanoparticles": Attractive Intermolecular Interactions Stabilize Specific Ligand Ratios on the Surfaces of Nanoparticles

*Zonglin Chu, Yanxiao Han, Petr Král, and Rafal Klajn**

Abstract: *Confining organic molecules to the surfaces of inorganic nanoparticles can induce intermolecular interactions between them, which can affect the composition of the mixed self-assembled monolayers obtained by co-adsorption from solution of two different molecules. Two thiolated ligands (a dialkylviologen and a zwitterionic sulfobetaine) that can interact with each other electrostatically were coadsorbed onto gold nanoparticles. The nanoparticles favor a narrow range of ratios of these two molecules that is largely independent of the molar ratio in solution. Changing the solution molar ratio of the two ligands by a factor of 5000 affects the on-nanoparticle ratio of these ligands by only threefold. This behavior is reminiscent of the formation of insoluble inorganic salts (such as AgCl), which similarly compensate positive and negative charges upon crystallizing. Our results pave the way towards developing well-defined hybrid organic–inorganic nanostructures.*

The properties of inorganic nanoparticles (NPs) can be fine-tuned by decorating their surfaces with binary rather than single-component monolayers of organic ligands. Engineering the composition of these "mixed" self-assembled monolayers (mSAMs) has proven important for applications in sensing[1,2] (including by surface-enhanced Raman scattering[3,4]), catalysis,[5,6] and nanomedicine.[7–9] The nanoscale architecture of mSAMs affects the way NPs self-assemble[10–12] and it is critical for efficient reversible isomerization of immobilized molecular switches.[13,14] Unfortunately, predicting the composition of mSAMs is not an easy task, and the assumption that the molar ratio of ligands in solution will be preserved on NPs is often wrong.[15–17] The discrepancy between the solution ratio and the surface ratio can stem from intermolecular interactions between the ligands,[18,19] solvation effects,[20] the steric bulkiness of the ligands,[21,22] and so on. Herein, we studied the competitive adsorption of two novel thiol ligands onto gold NPs. In solution, these thiols are solvated and do not interact with each other. Adsorption onto NPs, however, activates electrostatic interactions between them, which are maximized at a particular ratio of the two ligands. Consequently, the NPs onto which the ligands co-adsorb favor a narrow range of ratios of these two molecules that is largely independent of the molar ratio in solution. We show that the molar fraction of a ligand can be enriched by as much as 150 times upon the transfer from the solution onto NPs. This behavior is reminiscent of the precipitation of inorganic salts (for example, AgCl), which similarly compensate positive and negative charges upon crystallizing.

Our experiments were motivated by developing redox-responsive NPs. Whereas light-responsive nanomaterials are increasingly abundant,[23–28] examples of NPs whose properties can be controlled using redox stimuli are relatively scarce and are limited to organic solvents.[29,30] We hypothesized that redox-responsive NPs compatible with aqueous environments could be obtained by functionalizing gold NPs with viologen-terminated thiol **1**, whereby the number of ligands of **1** per NP could be controlled by co-adsorption with varying amounts of a redox-inactive, sulfobetaine[31,32]-based ligand **2**. To this end, we functionalized 5.9 nm gold NPs with different mixtures of **1** and **2**, where the molar fraction of **1** in the initial solution, that is, $n_1/(n_1+n_2)$, is denoted as θ (Figure 1). In a typical experiment, dodecylamine-capped NPs in chloroform were treated with a solution of **1** + **2** in methanol/DMSO (a tenfold

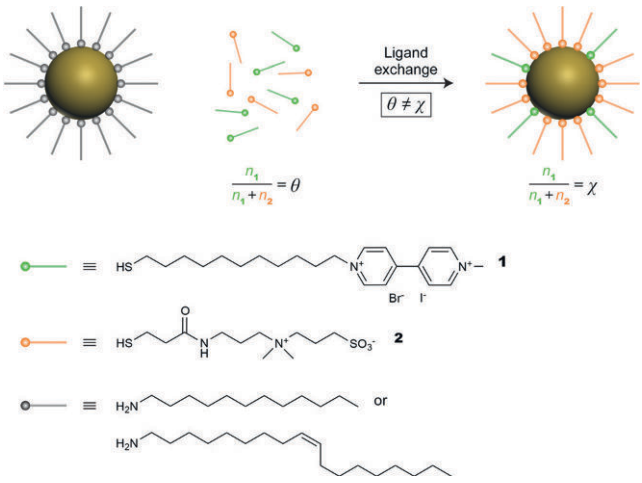


Figure 1. Representation of a ligand exchange reaction on nanoparticles (NPs) involving a mixture of two incoming thiol ligands. The molar fraction of thiol **1** in the initial solution is denoted as θ and on the resulting NPs as χ.

[*] Dr. Z. Chu, Prof. Dr. R. Klajn
Department of Organic Chemistry, Weizmann Institute of Science
Rehovot, 76100 (Israel)
E-mail: rafal.klajn@weizmann.ac.il
Y. Han, Prof. Dr. P. Král
Department of Chemistry, University of Illinois at Chicago
Chicago, IL 60607 (USA)
Prof. Dr. P. Král
Department of Physics, Department of Biopharmaceutical Sciences, University of Illinois at Chicago
Chicago, IL 60607 (USA)
Supporting information and the ORCID identification number(s) for the author(s) of this article can be found under: https://doi.org/10.1002/anie.201800673.

 © 2018 Wiley-VCH Verlag GmbH & Co. KGaA, Weinheim

excess of thiols with respect to the number of binding sites on the NPs was used), resulting in slow precipitation of thiolated NPs (see the Supporting Information, Section 3.1 for details). The precipitates were washed copiously to remove the excess of small molecules and dried. NPs functionalized with pure **1** or **2** (that is, $\theta = 0$ or 1) were readily soluble in pure water, whereas those co-functionalized with mSAMs comprising **1** and **2** were soluble only for $\theta > 0.25$. All of the particles were soluble in water containing NaCl (0.5 M), which can screen the electrostatic interactions (see also the discussion in Supporting Information, Section 4). We verified by transmission electron microscopy (TEM) that the place-exchange reaction did not affect the size and size distribution of the NPs.

To characterize **1**/**2**-functionalized NPs, we first performed zeta (ζ) potential measurements. We found that NPs functionalized with pure **2** (i.e., $\theta = 0$) exhibited a highly negative ζ-potential of -27.9 ± 2.0 mV, in agreement with these particles having their outer surfaces decorated with the negatively charged sulfonate groups. Similarly, **1**-functionalized NPs ($\theta = 1$) exhibited a highly positive ζ-potential of $+54.4 \pm 2.2$ mV. Surprisingly, however, the ζ-potentials of $0.25 < \theta < 1$ NPs showed little dependence on θ and ranged between $+28.6 \pm 1.0$ mV (for $\theta = 0.25$) and $+37.1 \pm 2.4$ mV ($\theta = 0.80$), suggesting that the molar fraction of **1** on nanoparticles (which we denote as χ) remains rather constant and is largely independent of the molar fraction in the solution used for NP functionalization (that is, $\chi \neq \theta$; Figure 1).

To better understand these results, we developed a procedure for estimating χ based on ^{1}H NMR spectroscopy. We took advantage of the fact that the NMR peaks of aromatic protons of **1** ($\delta \approx 9.3$–8.7 ppm) and methyl protons of **2** (ca. 3.15 ppm) do not overlap with any of the other ligand's peaks (Supporting Information, Figures S8 and S18, respectively), and that integrating them could be used to determine the molar fraction of each ligand on the NPs. Upon attachment to the NPs, significant line broadening in the NMR spectra was observed, which could be attributed to the restricted molecular motion of immobilized molecules, as reported previously.[33–36] To overcome this difficulty, we liberated thiols **1** and **2** to solution (in the form of the corresponding disulfides) by etching the NPs with molecular iodine[37–39] in deuterated solvents (see Supporting Information, Section 3.4.1). Analysis of the resulting NMR spectra confirmed that the molar fraction of **1** on the NPs (χ) shows little dependence on the fraction of **1** in solution (θ). For example, increasing θ from 0.05 to 0.80 (that is, by a factor of 16) led to an only a 2.2-fold increase in χ. Overall, the dependence of χ on θ followed a roughly linear curve with a slope of about 0.15 (see the red data points in Figure 2c), which indicates that NPs have a propensity to stabilize a narrow range of **1**:**2** ratios, suggesting the presence of attractive electrostatic interactions between immobilized **1** and **2**.

To corroborate this reasoning, we studied the competitive adsorption of **1** and **2** on gold NPs by means of atomistic molecular dynamics (MD) simulations. In these studies, we placed a 5.5 nm gold NP protected with a submonolayer of **1** + **2** ($\chi = 0.205$; overall 400 ligands; densely packed monolayer comprises 444 ligands) in a solution containing an excess of both thiols, and calculated the distributions of **1** vs. **2** at increasing distances from the NP surface (for details, see the Supporting Information, Section 5). We found that the **2**:**1** ratio was enriched near the NP surfaces for all **2**:**1** molar ratios in the solution. For example, Figure 3a shows the distribution of **1** and **2** around a $\chi = 0.205$ gold NP immersed in chloroform containing equal amounts of both thiols, where we found that the **2**:**1** ratio within 2.75 nm of the NP surface increased from 50 to 65 % (Figure 3b). To further confirm the presence of attractive interactions between **1** and **2**, we

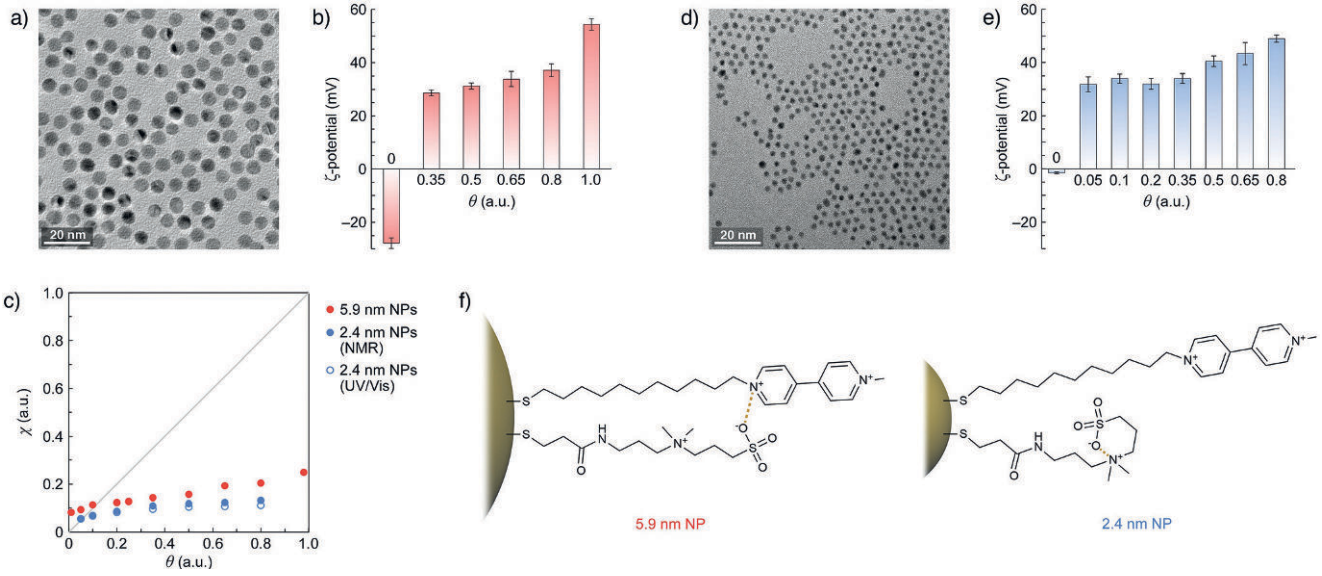


Figure 2. a) A representative TEM image of 5.9 nm gold NPs. b) ζ-potentials of 5.9 nm gold NPs functionalized with mixtures of **1** and **2** as a function of θ. c) χ as a function of θ for 5.9 nm (red) and 2.4 nm (blue) gold NPs estimated using NMR (solid markers) and UV/Vis absorption spectroscopy (empty markers). The gray line corresponds to $\theta = \chi$. d) A representative TEM image of 2.4 nm gold NPs. e) ζ-potentials of 2.4 nm gold NPs functionalized with mixtures of **1** and **2** as a function of θ. f) Proposed modes of dominating inter- and intramolecular electrostatic interactions on 5.9 nm (left) and 2.4 nm (right) NPs.

© 2018 Wiley-VCH Verlag GmbH & Co. KGaA, Weinheim

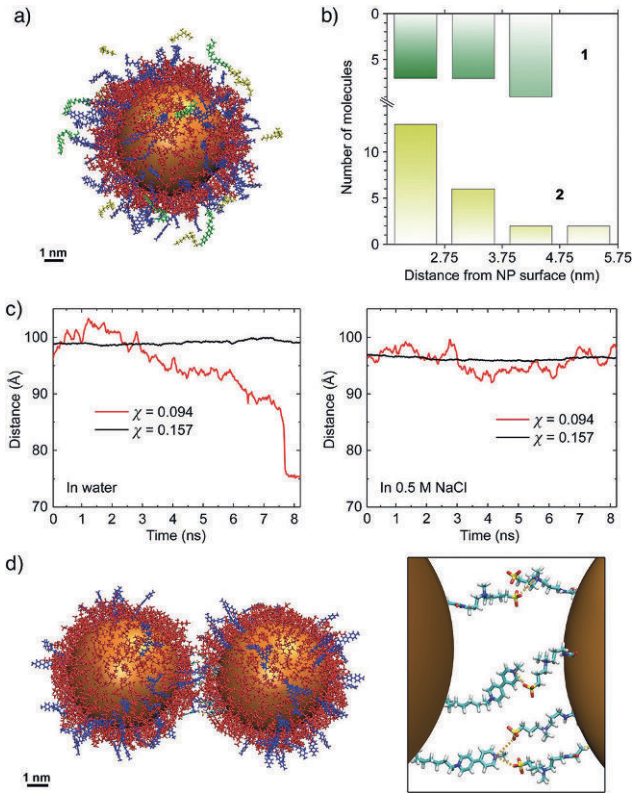


Figure 3. a) Snapshot from molecular dynamics (MD) simulations of a 5.5 nm gold NP functionalized with a sub-monolayer of **1** (blue) and **2** (red) at $\chi = 0.205$ (total 400 thiol ligands) in a solution containing 23 molecules of **1** and 23 molecules of **2** in explicit chloroform (chloroform molecules omitted for clarity). Free **1** and **2** located within the initial 2.75 nm of the NP surface are shown in green and yellow, respectively. b) Calculated distributions of **1** (green) and **2** (yellow) at increasing distances from the NP surface around 5.5 nm gold NPs treated with 23 molecules of **1** and 23 molecules of **2**. c) Distance between the centers of two **1**/**2**-functionalized 5.5 nm NPs (at two different **1**:**2** molar ratios) placed in water (left) and a salt solution (right) as a function of time. d) Snapshot from MD simulations of two **1**/**2**-functionalized 5.5 nm gold NPs ($\chi = 0.094$) in water. The image on the right focuses on the intermolecular interactions between ligands adsorbed on the neighboring NPs.

investigated intermixing of the two ligands adsorbed on a 5.5 nm, $\chi = 0.205$ Janus NP (that is, having two faces, each functionalized with a single-component monolayer of either **1** or **2**). These simulations revealed that the ligands could readily migrate on the NP surface to increase the favorable interactions between the two compounds (Supporting Information, Section 5.3). Importantly, these interactions could be visualized directly using two-dimensional NMR spectroscopy. Distinct nuclear Overhauser (nOe) correlations between the upfield-shifted (alkyl) protons of **1** and N^+–C–**H** protons of **2** were observed (Supporting Information, Figure S32) in the ^{1}H–^{1}H NOESY spectra of **1**/**2**-functionalized 2.4 nm NPs, confirming that the two compounds are intermixed on the NP surfaces.

MD simulations were also employed to rationalize the solubility properties of **1**/**2**-functionalized NPs. The red trace in Figure 3c, left, shows the time dependence of the distance between the centers of two $\chi = 0.094$, 5.5 nm gold NPs placed in pure water; it can be seen that the particles aggregate within 8 ns. The snapshots shown in Figure 3d reveal that the aggregation is facilitated by electrostatic interactions between **1** and **2** adsorbed on the neighboring NPs. In contrast, the same two NPs placed in a 0.5 M NaCl solution remain stable indefinitely in the non-aggregated state (Figure 3c, right). Increasing the fraction of **1** to $\chi = 0.157$ renders the NPs colloidally stable in both pure water and salt solution (black lines in Figure 3c), in agreement with the experimental observations.

To further confirm that co-adsorption of **1** and **2** favors specific ligand ratios on the NPs, we worked with **1**+**2** mixtures containing a large excess of either ligand (see Supporting Information, Section 3.4.1.1). First, we subjected 5.9 nm NPs to a $\theta = 0.98$ mixture containing 68.6 equiv of **1** and 1.4 equiv of **2** (equiv with respect to the binding sites on the NPs) and found that the molar fraction of **1** on the functionalized NPs, $\chi = 0.25$ (that is, 0.25 equiv of **1** and 0.75 equiv of **2**). In other words, the efficiency of adsorption corresponded to about 0.36% and about 54% for **1** and **2**, respectively; that is, the adsorption of **2** was favored by a factor of about 150. However, when we started with a $\theta = 0.01$ mixture containing 0.5 equiv of **1** and 49.5 equiv of **2**, the selectivity was reversed: the resulting NPs ($\chi = 0.083$) hosted about 0.083 equiv of **1** and about 0.917 equiv of **2**, corresponding to adsorption efficiencies of about 16.6% and about 1.9% for **1** and **2**, respectively.

To ensure that the discrepancy between χ and θ does not originate from the tendency of particles to precipitate from the organic solution during NP functionalization, we prepared $\chi = 0.204$ NPs (obtained from a $\theta = 0.80$ mixture of **1** and **2**) and solubilized them in water. Incubating these NPs with the same $\theta = 0.80$ mixture of **1** and **2** in water did not markedly increase the fraction of **1** on the NPs ($\chi' = 0.213$ after 24 h in the presence of tenfold excess of free thiols in solution; Supporting Information, Section 3.4.1.2).

Next, we investigated the effect of NP size on the mutual stabilization of both ligands. To this end, we functionalized 2.4 nm gold NPs (Figure 2d; see also Supporting Information, Section 3.2) with different mixtures of **1** and **2**. Similar to 5.9 nm NPs, the smaller particles exhibited a narrow range of ζ-potentials (+32 to +49 mV; Figure 2e), and NMR analysis revealed that increasing θ by 16 times led to an only a 2.4-fold increase in χ (Figure 2c, solid blue markers). The molar fraction of **1** on 2.4 nm NPs could also be determined directly by UV/Vis spectroscopy (taking advantage of the high molar absorption coefficient of the viologen group in the UV region; see Supporting Information, Section 3.4.2) and the results closely matched those from NMR measurements (Figure 2c). Interestingly, however, we also found some notable differences between the large and the small NPs. First, the θ–χ dependence for 2.4 nm NPs deviated from the $\theta = \chi$ line (gray in Figure 2c) more markedly than for 5.9 nm NPs, indicating that the incorporation of **1** onto the smaller NPs is more disfavored. This result may appear surprising given that the larger curvature associated with the smaller NPs entails larger distances and therefore a smaller electrostatic repulsion between the like-charged viologen groups. Second, ζ-potential values of 2.4 nm NPs at a given χ value are significantly

 © 2018 Wiley-VCH Verlag GmbH & Co. KGaA, Weinheim

higher than those of 5.9 nm NPs, suggesting that the positive charges of the viologen groups on the larger particles are partially screened, possibly by engaging in intermolecular interactions with **2**. Third, the smaller NPs exhibited excellent solubility in water irrespective of the **1**/**2** ratio, whereas the larger NPs coated with mSAMs were only soluble above a critical fraction of **1** ($\chi > \approx 0.13$). Fourth, ζ-potential measurements on 2.4 nm NPs functionalized with pure **2** showed they have virtually no surface charge ($\zeta = -1.6 \pm 0.4$ mV, compared with -27.9 ± 2.0 mV for 5.9 nm NPs), which we confirmed by performing gel electropheresis experiments (see Supporting Information, Section 6). Together, these observations led us to conclude that decreasing the NP size results in a larger number of **2** forming an intramolecular salt bridge rather than exposing the terminal sulfonate group to the solution and/or making it available for intermolecular interactions with **1** (Figure 2 f, right and left, respectively).

Finally, we attempted to establish that the observed phenomenon is not limited to ligands **1** and **2**. To this end, we synthesized additional five thiols **3**–**7**, each containing a positively or a negatively charged group, and investigated their co-adsorption onto gold nanoparticles (Supporting Information, Section 7). The results of these studies showed that whereas the dependence of χ on θ was particularly weak for the **1**/**2** combination (most likely because of two positive charges and consequently strong electrostatic interactions involving **1**), the phenomenon was general and applicable to different charged groups (for example, pyridinium and tetraalkylammonium) and ligand lengths.

In summary, we found that co-adsorption of a positively charged viologen-based ligand and a zwitterionic sulfobetaine ligand onto metallic nanoparticles favors a narrow range of molar ratios of these two ligands on the functionalized particles. Molecular dynamics simulations revealed that this result could be attributed to attractive electrostatic interactions between the two ligands upon adsorption onto the NPs. Additional studies involving other charged thiols showed that the phenomenon is general and not limited to viologen-/sulfobetaine-based ligands. Interestingly, our results are complementary to those of Bishop of co-workers, who found that co-adsorption of ligands exhibiting repulsive interactions (polar and nonpolar) favors the formation of Janus NPs decorated with single-component patches of each ligand.[40] Our results are important in the context of attaining a fundamental understanding of self-assembly on nanostructured and planar surfaces as well as self-assembly in solution[41] and they pave the way towards developing novel redox-responsive nanomaterials.

Acknowledgements

This work was supported by the European Research Council (grant No. 336080 to R.K.), the Israel Ministry of Science (China-Israel cooperation, grant 3-13555 to R.K.), and the NSF (Division of Materials Research, grant No. 1506886 to P.K.). Z.C. acknowledges support from the Planning and Budgeting Committee of the Council for Higher Education, the Koshland Foundation, and a McDonald-Leapman grant. We gratefully acknowledge Dr. Liat Avram and Dr. Tong Bian for their assistance with NMR experiments and gel electrophoresis, respectively.

Conflict of interest

The authors declare no conflict of interest.

Keywords: ligand exchange · nanoparticles · self-assembly · supramolecular chemistry · surface chemistry

How to cite: *Angew. Chem. Int. Ed.* **2018**, *57*, 7023–7027
Angew. Chem. **2018**, *130*, 7141–7145

[1] E. S. Cho, J. Kim, B. Tejerina, T. M. Hermans, H. Jiang, H. Nakanishi, M. Yu, A. Z. Patashinski, S. C. Glotzer, F. Stellacci, B. A. Grzybowski, *Nat. Mater.* **2012**, *11*, 978–985.
[2] S. Yapar, M. Oikonomou, A. H. Velders, S. Kubik, *Chem. Commun.* **2015**, *51*, 14247–14250.
[3] G. F. Wang, H. Y. Park, R. J. Lipert, *Anal. Chem.* **2009**, *81*, 9643–9650.
[4] M. Gellner, K. Kömpe, S. Schlücker, *Anal. Bioanal. Chem.* **2009**, *394*, 1839–1844.
[5] M. Moreno, F. J. Ibanez, J. B. Jasinski, F. P. Zamborini, *J. Am. Chem. Soc.* **2011**, *133*, 4389–4397.
[6] G. Pieters, L. J. Prins, *New J. Chem.* **2012**, *36*, 1931–1939.
[7] A. Verma, F. Stellacci, *Small* **2010**, *6*, 12–21.
[8] M. Zheng, X. Y. Huang, *J. Am. Chem. Soc.* **2004**, *126*, 12047–12054.
[9] X. Liu, H. Li, Q. Jin, J. Ji, *Small* **2014**, *10*, 4230–4242.
[10] G. A. DeVries, M. Brunnbauer, Y. Hu, A. M. Jackson, B. Long, B. T. Neltner, O. Uzun, B. H. Wunsch, F. Stellacci, *Science* **2007**, *315*, 358–361.
[11] H. Kim, R. P. Carney, J. Reguera, Q. K. Ong, X. Liu, F. Stellacci, *Adv. Mater.* **2012**, *24*, 3857–3863.
[12] S. Borsley, E. R. Kay, *Chem. Commun.* **2016**, *52*, 9117–9120.
[13] T. Moldt, D. Brete, D. Przyrembel, S. Das, J. R. Goldman, P. K. Kundu, C. Gahl, R. Klajn, M. Weinelt, *Langmuir* **2015**, *31*, 1048–1057.
[14] P. K. Kundu, S. Das, J. Ahrens, R. Klajn, *Nanoscale* **2016**, *8*, 19280–19286.
[15] J. F. Hicks, F. P. Zamborini, A. Osisek, R. W. Murray, *J. Am. Chem. Soc.* **2001**, *123*, 7048–7053.
[16] C. A. Simpson, A. C. Agrawal, A. Balinski, K. M. Harkness, D. E. Cliffel, *ACS Nano* **2011**, *5*, 3577–3584.
[17] S. M. Bradford, E. A. Fisher, M.-V. Meli, *Langmuir* **2016**, *32*, 9790–9796.
[18] A. M. Kalsin, B. Kowalczyk, P. Wesson, M. Paszewski, B. A. Grzybowski, *J. Am. Chem. Soc.* **2007**, *129*, 6664–6665.
[19] M. Şologan, C. Cantarutti, S. Bidoggia, S. Polizzi, P. Pengo, L. Pasquato, *Faraday Discuss.* **2016**, *191*, 527–543.
[20] H. Choo, E. Cutler, Y.-S. Shon, *Langmuir* **2003**, *19*, 8555–8559.
[21] R. S. Ingram, M. J. Hostetler, R. W. Murray, *J. Am. Chem. Soc.* **1997**, *119*, 9175–9178.
[22] A. M. Smith, L. E. Marbella, K. A. Johnston, M. J. Hartmann, S. E. Crawford, L. M. Kozycz, D. S. Seferos, J. E. Millstone, *Anal. Chem.* **2015**, *87*, 2771–2778.
[23] A. Manna, P.-L. Chen, H. Akiyama, T. X. Wei, K. Tamada, W. Knoll, *Chem. Mater.* **2003**, *15*, 20–28.
[24] R. Klajn, K. J. M. Bishop, B. A. Grzybowski, *Proc. Natl. Acad. Sci. USA* **2007**, *104*, 10305–10309.
[25] C. Raimondo, F. Reinders, U. Soydaner, M. Mayor, P. Samorì, *Chem. Commun.* **2010**, *46*, 1147–1149.

 © 2018 Wiley-VCH Verlag GmbH & Co. KGaA, Weinheim

[26] D. Liu, W. Chen, K. Sun, K. Deng, W. Zhang, Z. Wang, X. Jiang, *Angew. Chem. Int. Ed.* **2011**, *50*, 4103 – 4107; *Angew. Chem.* **2011**, *123*, 4189 – 4193.
[27] D. Manna, T. Udayabhaskararao, H. Zhao, R. Klajn, *Angew. Chem. Int. Ed.* **2015**, *54*, 12394 – 12397; *Angew. Chem.* **2015**, *127*, 12571 – 12574.
[28] H. He, M. Feng, Q. Chen, X. Zhang, H. Zhan, *Angew. Chem. Int. Ed.* **2016**, *55*, 936 – 940; *Angew. Chem.* **2016**, *128*, 948 – 952.
[29] R. Klajn, L. Fang, A. Coskun, M. A. Olson, P. J. Wesson, J. F. Stoddart, B. A. Grzybowski, *J. Am. Chem. Soc.* **2009**, *131*, 4233 – 4235.
[30] M. A. Olson, A. Coskun, R. Klajn, L. Fang, S. K. Dey, K. P. Browne, B. A. Grzybowski, J. F. Stoddart, *Nano Lett.* **2009**, *9*, 3185 – 3190.
[31] J. G. Weers, J. F. Rathman, F. U. Axe, C. A. Crichlow, L. D. Foland, D. R. Scheuing, R. J. Wiersema, A. G. Zielske, *Langmuir* **1991**, *7*, 854 – 867.
[32] Z. Chu, Y. Feng, *Langmuir* **2012**, *28*, 1175 – 1181.
[33] L. E. Marbella, J. E. Millstone, *Chem. Mater.* **2015**, *27*, 2721 – 2739.
[34] A. Badia, W. Gao, S. Singh, L. Demers, L. Cuccia, L. Reven, *Langmuir* **1996**, *12*, 1262 – 1269.
[35] A. C. Templeton, S. Chen, S. M. Gross, R. W. Murray, *Langmuir* **1999**, *15*, 66 – 76.
[36] B. S. Zelakiewicz, A. C. de Dios, Y. Tong, *J. Am. Chem. Soc.* **2003**, *125*, 18 – 19.
[37] M. P. Rowe, K. E. Plass, K. Kim, Ç. Kurdak, E. T. Zellers, A. J. Matzger, *Chem. Mater.* **2004**, *16*, 3513 – 3517.
[38] H. Zhou, X. Li, A. Lemoff, B. Zhang, B. Yan, *Analyst* **2010**, *135*, 1210 – 1213.
[39] E. A. Fisher, S. J. Duffy, M.-V. Meli, *RSC Adv.* **2015**, *5*, 33289 – 33293.
[40] D. M. Andala, S. H. R. Shin, H.-Y. Lee, K. J. M. Bishop, *ACS Nano* **2012**, *6*, 1044 – 1050.
[41] E. W. Kaler, K. L. Herrington, A. Kamalakara Murthy, J. A. N. Zasadzinski, *J. Phys. Chem.* **1992**, *96*, 6698 – 6707.

Manuscript received: January 17, 2018
Revised manuscript received: March 13, 2018
Accepted manuscript online: April 19, 2018
Version of record online: May 15, 2018

 © 2018 Wiley-VCH Verlag GmbH & Co. KGaA, Weinheim